Polymeric surfactants at liquid–liquid interfaces: Dependence of structural and thermodynamic properties on copolymer architecture

The Journal of Chemical Physics

RESEARCH ARTICLE | FEBRUARY 06 2024

Polymeric surfactants at liquid–liquid interfaces: Dependence of structural and thermodynamic properties on copolymer architecture

Jonathan G. Coldstream ; Philip J. Camp ; Daniel J. Phillips ; Peter J. Dowding

J. Chem. Phys. 160, 054902 (2024)
https://doi.org/10.1063/5.0189156

The Journal of Chemical Physics ARTICLE pubs.aip.org/aip/jcp

Polymeric surfactants at liquid–liquid interfaces: Dependence of structural and thermodynamic properties on copolymer architecture

Cite as: J. Chem. Phys. 160, 054902 (2024); doi: 10.1063/5.0189156
Submitted: 27 November 2023 • Accepted: 11 January 2024 •
Published Online: 6 February 2024

Jonathan G. Coldstream,[1,a)] Philip J. Camp,[1,b)] Daniel J. Phillips,[2] and Peter J. Dowding[2]

AFFILIATIONS

[1] School of Chemistry, University of Edinburgh, David Brewster Road, Edinburgh EH9 3FJ, Scotland
[2] Infineum UK Ltd., P.O. Box 1, Milton Hill, Abingdon OX13 6BB, United Kingdom

[a)] **Author to whom correspondence should be addressed:** jonathan.coldstream@ed.ac.uk
[b)] **Electronic mail:** philip.camp@ed.ac.uk

ABSTRACT

Polymeric surfactants are amphiphilic molecules with two or more different types of monomers. If one type of monomer interacts favorably with a liquid, and another type of monomer interacts favorably with another, immiscible liquid, then polymeric surfactants adsorb at the interface between the two liquids and reduce the interfacial tension. The effects of polymer architecture on the structural and thermodynamic properties of the liquid–liquid interface are studied using molecular simulations. The interface is modeled with a non-additive binary Lennard-Jones fluid in the two-phase region of the phase diagram. Block and gradient copolymer surfactants are represented with coarse-grained, bead-spring models, where each component of the polymer favors one or the other liquid. Gradient copolymers have a greater concentration at the interface than do block copolymers because the gradient copolymers adopt conformations partially aligned with the interface. The interfacial tension is determined as a function of the surface excess of polymeric surfactant. Gradient copolymers are more potent surfactants than block copolymers because the gradient copolymers cross the dividing surface multiple times, effectively acting as multiple individual surfactants. For a given surface excess, the interfacial tension decreases monotonically when changing from a block to a gradient architecture. The coarse-grained simulations are complemented by all-atom simulations of acrylic-acid/styrene copolymers at the chloroform-water interface, which have been studied in experiments. The agreement between the simulations (both coarse-grained and atomistic) and experiments is shown to be excellent, and the molecular-scale structures identified in the simulations help explain the variation of surfactancy with copolymer architecture.

I. INTRODUCTION

Surfactants are molecules containing both solvophilic and solvophobic moieties and are often used because of their ability to self-assemble, encapsulate species, adsorb at interfaces, reduce interfacial tension, modify other surface properties, and stabilize various types of emulsions. Their applications span a wide variety of uses from emulsion stability in food,[1] to detergents,[2] friction reduction,[3] and enhanced oil recovery.[4] Amphiphilic polymers, in particular, have been identified as candidates for drug delivery,[5] as polymeric electrolytes in battery technologies,[6,7] and as emulsion stabilizers.[8,9] The potential of polymeric surfactants is high due to the broad ranges of chemical composition and architecture, which can be tailored to fit a specific application. Copolymer properties can vary hugely based on the choices of monomers,[10] molecular weight,[11] and polymer architecture.[12–14]

One simple choice of copolymer architecture is a block copolymer, consisting of two or more homopolymers bonded together. Another choice is a gradient copolymer, where the monomer composition changes smoothly over the length of the chain. In general, amphiphilic gradient copolymers have properties very different from those of the equivalent block copolymer, showing broad glass transition temperatures,[15,16] greater sensitivity to temperature and pH,[14,17,18] and different interfacial behavior. Interfacial behavior, in the context of lamellar segregation, has been studied using self-consistent field theory alongside experiment, showing how

the structure of the melt interface can be controlled by altering the monomer sequence.[19–21] Gradient copolymers are also better compatibilizers of immiscible homopolymer blends, stabilizing smaller droplets against coalescence.[22] Such properties are important in modern plastic recycling methods, allowing otherwise immiscible polymers to be formed into composite functional materials.[23] Symmetric diblock copolymers cannot fulfill the same function as the critical micelle concentrations are too low, meaning that the polymers are trapped in micelles, and not active at interfaces.[24]

While the behavior of copolymers at the interfaces of immiscible melts has received much attention, the properties at liquid–liquid interfaces have received comparatively little, particularly in relation to gradient copolymers. Asymmetric, ionic block copolymers, with one short block and one long block, have been shown to be interfacially active, with the degree of adsorption and structure depending on the charge fraction on the polymer.[25] Yuan *et al.* showed that modifying the water–chloroform interface with an acrylic-acid/styrene gradient copolymer reduced the interfacial tension much more than the equivalent block copolymer.[26] Yuan *et al.* proposed the higher critical micelle concentration, and polymer conformations aligned along the interface, as the primary reasons for the greater interfacial activity of the gradient copolymer. Block copolymers, by contrast, have low critical micelle concentrations, and individual molecules are preferentially aligned perpendicular to the interface, with each block fully solvated in its respective good solvent.

In this work, a bead-spring model of polymers, a non-additive binary Lennard-Jones (LJ) fluid, and Langevin-dynamics simulations are used to study the behaviors of block and gradient copolymers adsorbed at the liquid–liquid interface, with a focus on how polymer structure can alter the interfacial tension. Copolymer sequences are varied systematically from a block copolymer to a copolymer with a linear composition profile, resulting in systematic changes in the interfacial tension for a given amount of polymers adsorbed at the interface. All-atom simulations are carried out for acrylic-acid/styrene polymers adsorbed at the water–chloroform interface, to match up with experiments.[26] The basic picture of parallel conformations of gradient copolymers, and perpendicular conformations of block copolymers, with respect to the liquid–liquid interface, is confirmed in the coarse-grained and all-atom simulations. The coarse-grained and atomistic simulations are compared to each other, and to experimental data, showing good agreement. Comparisons are made with prescribed surface excesses of polymers so that bulk-solution self-assembly and the kinetics of the surface adsorption from the bulk solution need not be considered.

The rest of this article is organized as follows. The bead-spring and all-atom models and methods are defined, respectively, in Sec. II A and Sec. II B. The specific copolymer sequences are defined in Sec. II C, and the relevant structural and thermodynamic properties of the systems are introduced in Sec. II D. The results are presented in Sec. III, and Sec. IV concludes this article.

II. SIMULATION MODELS AND METHODS

The two types of models used in this article are outlined in this section. The first is a coarse-grained model consisting of bead-spring polymers suspended in a phase-separated binary LJ fluid, which models a symmetric liquid–liquid interface. The second is an all-atom model of acrylic-acid/styrene polymers at the water–chloroform interface, based on the OPLS force field.[27–29]

A. Coarse-grained simulations

The majority of simulations performed here use a bead-spring model of a polymer.[30] Above a certain characteristic length scale, the Kuhn length, the structural properties of a polymer follow simple scaling laws and do not depend on details at the atomic level.[31] This allows the microscopic structure of the polymer to be ignored in favor of increased computational performance. Variations on the bead-spring model have been used to study the properties of polymer melts and blends,[30,32–35] surface adsorption,[36–38] and polymers in solution.[39,40]

The bead-spring model is adapted to adsorption at the liquid–liquid interface by modeling the solvents explicitly as immiscible LJ fluids. The LJ potential is given by

$$V_{\mathrm{LJ}}(r) = 4\varepsilon\left[\left(\frac{\sigma}{r}\right)^{12} - \left(\frac{\sigma}{r}\right)^{6}\right], \tag{1}$$

where ε is the well depth (which depends on particle type) and σ is the diameter of the particle (the same in all cases). The solvents are composed of two particle types, type A and type B. Like solvent particles interact with $\varepsilon^{\mathrm{SS}}_{\mathrm{AA}} = \varepsilon^{\mathrm{SS}}_{\mathrm{BB}} = \varepsilon^{\mathrm{SS}}$; the superscripts denote where the particles are (S for solvent), and the subscripts denote the particle types. Unlike solvent particles interact with $\varepsilon^{\mathrm{SS}}_{\mathrm{AB}} = \varepsilon^{\mathrm{SS}}_{\mathrm{BA}} = \alpha\varepsilon^{\mathrm{SS}}$, with $\alpha \le 1$. The demixing phase diagram of the non-additive, binary LJ fluid is known,[41] and this informed the choice of α, detailed below.

The polymer consists of N_{m} "monomer" beads of diameter σ, with adjacent beads connected by a finitely extensible nonlinear elastic (FENE) potential,

$$V_{\mathrm{FENE}}(r) = -\frac{1}{2}kR_0^2 \ln\left[1 - \left(\frac{r}{R_0}\right)^2\right], \tag{2}$$

where k is a spring constant and R_0 is the maximum extension of the bond. The FENE potential is used instead of a harmonic spring to prevent crossing of polymer chains, given a small enough value of R_0. Like polymer beads interact via LJ potentials with $\varepsilon^{\mathrm{PP}}_{\mathrm{AA}} = \varepsilon^{\mathrm{PP}}_{\mathrm{BB}} = \varepsilon^{\mathrm{PP}}$; the superscripts denote that the particles are in the polymer (P). Unlike interactions have $\varepsilon^{\mathrm{PP}}_{\mathrm{AB}} = \varepsilon^{\mathrm{PP}}_{\mathrm{BA}} = \beta\varepsilon^{\mathrm{PP}}$, where $\beta \le 1$. The cross interaction between a bead in a polymer and a bead in a solvent is given by the geometric mean of the polymer–polymer and solvent–solvent interactions. With these choices, and particularly with $\alpha, \beta < 1$, liquid A is a good solvent for the polymer A beads, and liquid B is a good solvent for the polymer B beads. For simplicity, this study is restricted to beads with equal diameter σ, equal mass m, and equal like-particle interaction energy parameters $\varepsilon^{\mathrm{SS}} = \varepsilon^{\mathrm{PP}} = \varepsilon$; the relative strengths of solvent–solvent and polymer–polymer interactions could be tuned by removing the last restriction. All of the solvent and polymer interaction energy parameters are summarized in Table I. The polymer architectures are detailed separately in Sec. II C.

TABLE I. Summary of the LJ energy parameters between beads of types A and B in solvents (S) and in polymers (P). α and β are scaling factors for the AB interactions in solvents and polymers, respectively; here, $\alpha = \beta = 0.5$. In all cases, the SP interactions are given by the geometric means of the SS and PP interactions.

	SS	PP	SP and PS
AA	ε	ε	ε
BB	ε	ε	ε
AB and BA	$\alpha\varepsilon$	$\beta\varepsilon$	$\sqrt{\alpha\beta}\varepsilon$

All simulations were carried out under isothermal conditions using Langevin dynamics. The force on particle i at position vector $\boldsymbol{r}_i$ is given by

$$m\ddot{\boldsymbol{r}}_i = -\nabla_{\boldsymbol{r}_i} V - m\lambda\dot{\boldsymbol{r}}_i + \boldsymbol{\eta}_i(t), \tag{3}$$

where m is the mass of the particle, $V = \sum_{i<j} V_{ij}$ is the total potential energy, and λ is the friction coefficient. The white-noise, random force $\boldsymbol{\eta}_i(t)$ has zero mean and obeys the fluctuation–dissipation relation,

$$\langle \boldsymbol{\eta}_i(t) \cdot \boldsymbol{\eta}_j(t') \rangle = 6k_B T m\lambda\delta_{ij}\delta(t - t'), \tag{4}$$

where k_B is Boltzmann's constant and T is the temperature.

Coarse-grained simulations of polymers in immiscible liquids were run in the canonical (NVT) ensemble at a constant total bead density of $\rho^* = N_b\sigma^3/V = 0.8$, where $N_b = N_p N_m + N_s = 150\,000$ is the total number of beads, N_p is the number of polymers, $N_m = 128$ is the number of monomers per polymer (64 of each of type A and type B), N_s is the number of solvent beads ($N_s/2$ of each of A and B), and V is the simulation box volume. The box was cuboidal with $L_x = L_y = L_z/3$, and hence, $L_x = L_y = 39.685\sigma$ and $L_z = 119.055\sigma$. Periodic boundary conditions were applied in all three directions. The temperature was set to $T^* = k_B T/\varepsilon = 1$, and the friction coefficient in LJ units was set to $\lambda^* = 1$. The solvent non-additivity parameter was set to $\alpha = 0.5$, as this is known to give almost complete phase separation when $\rho^* = 0.8$ and $T^* = 1$.[41] The polymer non-additivity parameter, β, was set to the same value. All LJ potentials were cut and shifted at $r = 2.5\sigma$, and the maximum extension of the FENE potential was set to $R_0 = 1.5\sigma$. The equations of motion were integrated with a time step, in LJ units, of $\delta t^* = 0.01$. Systems were equilibrated for at least $3 \times 10^6 \delta t^*$, before a production run of $2 \times 10^6 \delta t^*$.

Initial configurations were generated with two slabs of pure liquid, and the interface oriented in the xy plane so that with the periodic boundary conditions, there are two liquid–liquid interfaces. Equal numbers of polymers were placed at the interfaces so that the surface excess was the same for each one. The surface excess was, therefore, $\Gamma^{ex} = N_p/2L_xL_y$ at each interface. Simulations were carried out with $N_p = 0, 10, 20, \ldots, 100$, giving reduced surface excesses up to $\Gamma^{ex}\sigma^2 \simeq 0.032$. Some test simulations were also carried out with completely random initial configurations to confirm that the two liquids phase separated spontaneously, and the block or gradient copolymers adsorbed to the resulting interfaces. Initial configurations were generated with PACKMOL,[42] and all simulations were performed using LAMMPS.[43–45]

B. All-atom simulations

All-atom simulations are much more computationally expensive than the coarse-grained ones and were used here on a few selected systems to check the reliability of the simpler model and to allow a more direct comparison with experiment. Acrylic-acid/styrene copolymers at the water–chloroform interface were modeled using the OPLS-AA force field.[27–29] The LJ interactions were cut-off at 12 Å, and the long-range Coulomb interactions were calculated using the particle–particle particle–mesh method. As with the coarse-grained simulations, initial configurations were generated with the interfaces preformed, and containing equal numbers of polymers. The numbers of water and chloroform molecules were chosen as 50 000 and 12 000, respectively, to give roughly equal volumes of the two coexisting phases. Again, some tests were performed from random starting configurations to confirm that interface formation and polymer adsorption were spontaneous processes. Simulations were performed in a cuboidal box with $L_x = L_y \ll L_z$, with L_z being large enough to avoid interactions between polymers at opposing interfaces, and with periodic boundary conditions applied in all three directions.

The all-atom simulations were prepared carefully so that the density and box shape were appropriate for a standard pressure $P = 1$ atm at $T = 23\,^{\circ}$C. First, simulations were run in the NVT ensemble for 0.25 ns with a timestep of 0.5 fs. The time step was then increased to 1 fs, and the system was propagated for a further 5 ns in the NPT ensemble, with the ratio of L_z to $L_x = L_y$ fixed at its initial value, and with isotropic scaling of the box volume. The box lengths in the x and y directions were then fixed at the average values from this NPT run. Another 5 ns run was performed with the barostat applied only in the z direction. The box length in the z direction was then fixed at the average from this last NPT run. Finally, a further 20 ns of equilibration was carried out in the NVT ensemble, followed by a production run of 10 ns. The point of this protocol was to prepare an NVT simulation in which the elements of the pressure tensor could be computed without any artificial coupling mediated by the barostat, box-length scaling, or volume-scaling. The Nosé–Hoover thermostat and barostat were used throughout. Initial configurations were generated using PACKMOL,[42] and simulations were run using LAMMPS.[43–45]

C. Polymer sequences

The composition profile along the polymer chain was described by the probability, $p_A(n)$, of a given bead at position $0 \le n \le N_m - 1$ in the chain being of type A,

$$p_A(n) = \frac{1}{2}\left\{1 + \frac{\mathrm{erf}\left[b\left(\frac{2n}{N_m - 1} - 1\right)\right]}{\mathrm{erf}\, b}\right\}. \tag{5}$$

The function is defined so that $p_A(0) = 0$ and $p_A(N_m - 1) = 1$. b is a "blockiness" parameter, where $b \to 0$ corresponds to a constant-gradient (or just "gradient") profile, and $b \to \infty$ corresponds to a step function, representing a block copolymer. Composition profiles with $b = 0$ (gradient), 1, 2, 4, and ∞ (block) are plotted in Fig. 1.

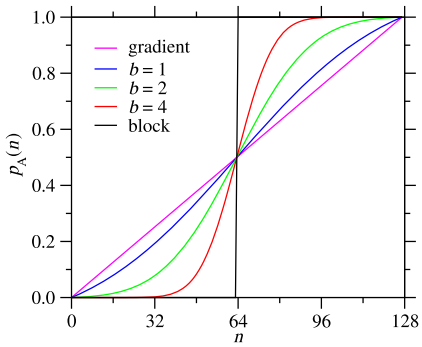

FIG. 1. The composition profile as a function of monomer number $0 \le n \le N_m - 1$ according to Eq. (5), with $N_m = 128$ and various values of b. The (constant) gradient and block profiles correspond to $b = 0$ and $b = \infty$, respectively.

D. Structural and thermodynamic properties

In the coarse-grained simulations, the structures of the liquid–liquid interfaces were characterized using local concentration profiles $\rho(z)$ for each type of solvent and polymer bead. Similar profiles were computed for the all-atom simulations by grouping atoms according to which liquid, and which monomer, they belong to.

The interfacial tension associated with one interface is given by[46]

$$\gamma = \int_{-\infty}^{\infty} [P_N(z) - P_T(z)]dz, \tag{6}$$

where $P_N = P_{zz}$ is the normal component of the pressure tensor, and $P_T = (P_{xx} + P_{yy})/2$ is the average transverse component. Since the instantaneous average of the pressure tensor within the simulation box is $\overline{P}_{\alpha\beta} = L_z^{-1} \int_0^{L_z} P_{\alpha\beta}(z)dz$, and this includes two interfaces, the interfacial tension was computed using

$$\gamma = \frac{1}{2} L_z \langle \overline{P}_N - \overline{P}_T \rangle, \tag{7}$$

where the angled brackets denote ensemble averages.

The coarse-grained model is symmetric, in the sense that all interactions are invariant with respect to A ↔ B. Hence, the concentration profiles of polymer A and B beads should be the mirror images of one another with respect to the position of an interface $\overline{z}$, and this can be taken as the average z coordinate of the polymer beads adsorbed at that interface. One way to characterize the orientation of the polymer with respect to the interface is to count how many times monomer-monomer bonds "cut" the interface: a polymer oriented perfectly perpendicular to the interface will cut it once, and a polymer roughly aligned with the interface will cut it many times. Given the z coordinates of two contiguous monomers, z_n and z_{n+1}, the bond between them crosses the interface if $\overline{z}$ is between z_n and z_{n+1}. Therefore, the fraction of bonds in a given polymer that crosses the interface can be defined as

$$f_\times = \frac{N_\times}{N_m - 1}, \tag{8}$$

where $N_\times$ is the number of bonds in a molecule crossing the interface and $N_m - 1$ is the total number of bonds in a molecule. As defined, $1/(N_m - 1) \le f_\times \le 1$, small values indicate perpendicular alignment of a chain with respect to the interface, and large values indicate parallel alignment.

III. RESULTS

A. Coarse-grained simulations

Results for the coarse-grained polymer model introduced in Sec. II A are presented here. To begin, the block copolymer ($b = \infty$) will be compared to the gradient one ($b = 0$). Figure 2 shows a simulation snapshot taken from the end of the production run of (a) block copolymers and (b) gradient copolymers with $\Gamma^{ex}\sigma^2 = 0.016$. The equilibrium structures consist of the phase-separated liquids, and all of the copolymers adsorbed at the liquid–liquid interface. Comparing Figs. 2(a) and 2(b), the adsorbed block copolymers form a visually broader layer than the gradient copolymers, but they are also less densely packed. The two segments of the block copolymer are entirely dissolved in their respective good solvents, due to the energy penalty of being in bad solvent, as represented by the non-additivity parameters $\alpha, \beta < 1$. An example of an individual block copolymer conformation is shown in Fig. 2(c).

In contrast, the gradient copolymer forms a more dense, less extended layer at the interface. The central region of the polymer, being a mixture of both bead types, adopts a parallel conformation aligned with the interface, in order to form contacts between the polymer beads and their respective good solvents. At either end of the polymer, where the sequence consists of almost entirely a single monomer type, the polymer becomes solvated in its favored liquid

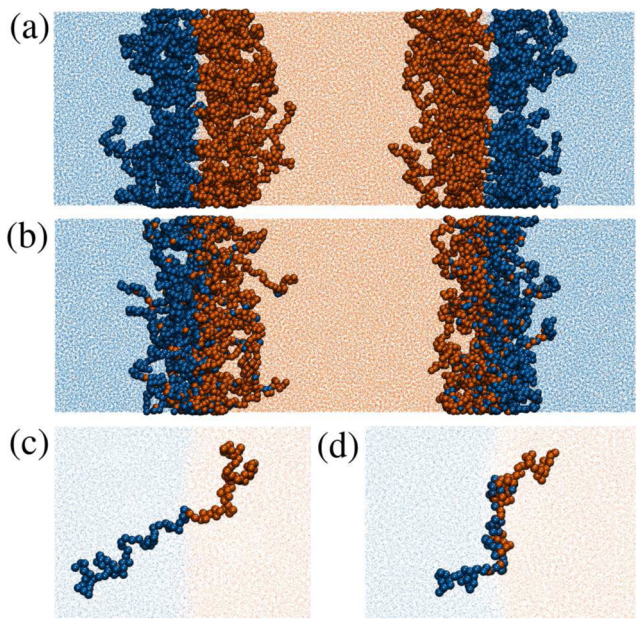

FIG. 2. Snapshots of (a) block copolymers at $\Gamma^{ex}\sigma^2 = 0.016$, (b) gradient copolymers at $\Gamma^{ex}\sigma^2 = 0.016$, (c) an enlarged configuration of a block copolymer from the system shown in (a), and (d) an enlarged configuration of a gradient copolymer from the system shown in (b).

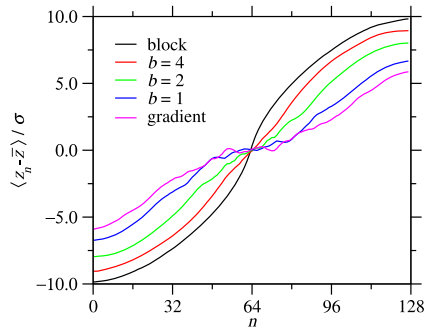

FIG. 3. The average distance of monomer n from the interface for block, gradient, and intermediate copolymers. The polymer surface excess is $\Gamma^{ex}\sigma^2 = 0.013$.

phase forming short coil-like tails. This effect allows a few polymer beads of type A to be solvated in liquid B, and vice versa. An example of the parallel conformation is shown in Fig. 2(d).

To quantify the differences between the block and gradient copolymer conformations, Fig. 3 shows the average position of a monomer i relative to the interface, $\langle z_n - \bar{z}\rangle$, where $\langle \bar{z}\rangle$ is taken as the position of the interface, as defined in Sec. II D. Results are shown for a surface excess of $\Gamma^{ex}\sigma^2 = 0.013$. A greater magnitude of $\langle z_n - \bar{z}\rangle$ implies that the bead at that position is more fully solvated in its respective good solvent. All of the profiles are symmetric about $n = (N_m - 1)/2$ due to the A ↔ B invariance of the interaction potentials. The block copolymer extends the furthest into the solvent as there is no energetic benefit of having more beads at the interface, resulting in the "perpendicular" structure shown in Fig. 2(c). At the other end of the blockiness spectrum, a central segment of each gradient copolymer, from approximately $n = 48$ to $n = 80$, is pinned to the liquid–liquid interface in the region $z_n \simeq \bar{z} \pm \sigma$. The central portion of the gradient sequence consists of a mixture of both bead types that favor opposing solvents, and so the polymer must adopt a "parallel" conformation at the interface to allow beads of each type to interact with the respective good solvent. As a large portion of the polymer is confined at the interface, this leaves shorter tails that extend, on average, to just over half as far into the solvent as the block copolymer. A representative snapshot of a gradient copolymer is shown in Fig. 2(d). Also shown in Fig. 3 are results for copolymers with blockiness parameters $b = 1$, 2, and 4. As b is increased, the parallel segments become shorter, and the fully solvated tails become longer.

Partial density profiles for beads in the block and gradient copolymers, at two different values of surface excess ($\Gamma^{ex}\sigma^2 = 0.0032$ and 0.016), are shown in Figs. 4(a)–4(d). All of the peaks are centered around $z \simeq 30\sigma$ and 90σ, which are the positions of the interfaces. The density profiles for the block copolymer show a single peak for each bead type, with only a small overlap between them. This is consistent with the simulation snapshots showing complete partitioning of the polymer blocks into the respective good solvents. The peaks are displaced a short distance from the interfaces, as the polymer minimizes the number of beads in the mixed interfacial region.

The partial density profiles for gradient copolymers are shown in Figs. 4(b) and 4(d). The most apparent difference, compared to

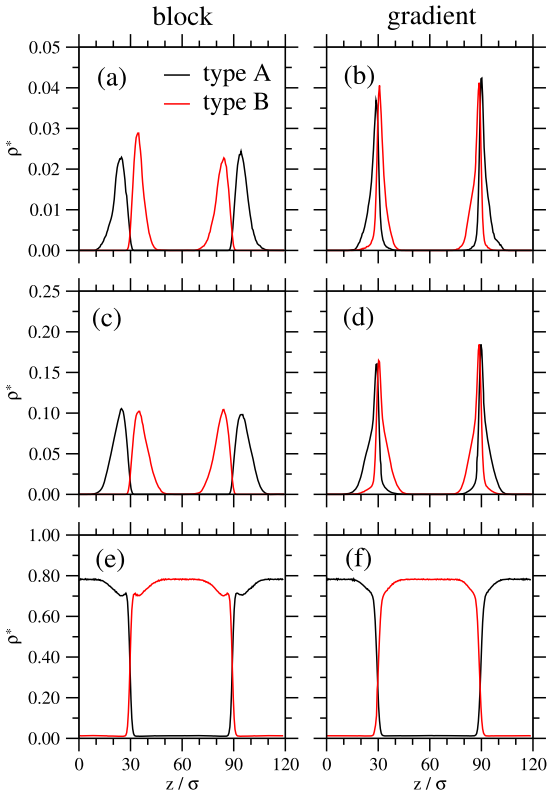

FIG. 4. (a)–(d) Density profiles $\rho^*(z) = \rho(z)\sigma^3$ along the axis perpendicular to the interface for block copolymers (left) and gradient copolymers (right), at different values of the surface coverage Γ^{ex}: (a) and (b) $\Gamma^{ex}\sigma^2 = 0.0032$ and (c) and (d) $\Gamma^{ex}\sigma^2 = 0.016$. (e) and (f) Density profiles of the solvent particles in systems with $\Gamma^{ex}\sigma^2 = 0.016$. Note the differences in scales on the y axes.

the block copolymer, is the larger peak positioned at the interface, due to the central segment of copolymer being aligned parallel with, and localized at, the interface. The density profiles for gradient copolymers show a significant overlap of bead types A and B. Individual beads surrounded by larger numbers of the opposite type, as occurs at the ends of the polymers, are able to be solvated in the bad solvent because the entropic penalty of confining a short section of the copolymer to the interface by loop formation outweighs the corresponding adsorption energy. The gradient copolymer density does not extend as far into the bulk phase as the block copolymer, which is consistent with the plots in Fig. 3.

Figures 4(e) and 4(f) show the solvent density profiles for the systems with $\Gamma^{ex}\sigma^2 = 0.016$. For the block copolymer, the local minima at $z/\sigma = 25$, 35, 85, and 95 in Fig. 4(e) correspond to the equivalent peaks in polymer density in Fig. 4(c). As the total density is roughly constant at $\rho^* = 0.8$ along the z-axis, the separation of the block-copolymer density peaks causes the characteristic local minima in the solvent density profiles. For the gradient copolymer, Fig. 4(f) does not show the equivalent local minima because the peaks in the copolymer density overlap at the interface.

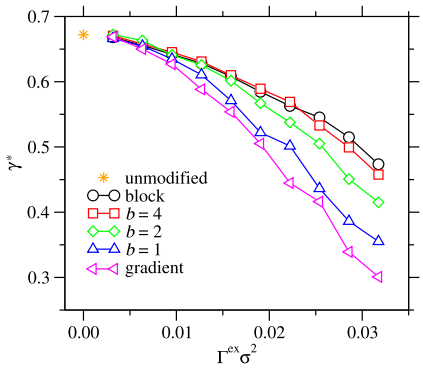

FIG. 5. The reduced interfacial tension $\gamma^* = \gamma\sigma^2/\varepsilon$ as a function of polymer surface excess $\Gamma^{ex}\sigma^2$ for block, gradient, and intermediate copolymers. The interfacial tension of the pure liquid–liquid interface is shown at $\Gamma^{ex}\sigma^2 = 0$.

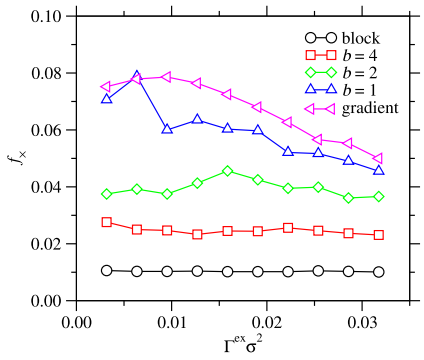

FIG. 6. The crossing fraction $f_\times$ plotted at various surface excesses of polymers $\Gamma^{ex}\sigma^2$ for block, gradient, and intermediate copolymers.

Figure 5 shows the reduced interfacial tension, $\gamma^* = \gamma\sigma^2/\varepsilon$, as a function of the reduced polymer surface excess, $\Gamma^{ex}\sigma^2$. The differences in polymer structuring at the interface have large effects on the interfacial tension. At low surface excess, all systems have a similar interfacial tension to the pure liquid–liquid interface. At high surface excess, the differences become clearer. At the highest value of $\Gamma^{ex}\sigma^2 \simeq 0.032$, the gradient copolymer system shows approximately double the reduction in interfacial tension than the block copolymer. This is due to the greater concentration of polymer beads at the interface in the gradient case. As shown already, the localization of the polymer at the interface can be controlled with the blockiness parameter b. Results for $b = 1$, 2, and 4 are also shown in Fig. 5, and they interpolate between the block and gradient cases. The overall conclusion here is that gradient copolymers are better surfactants than block copolymers, in the sense that they provide a greater reduction in interfacial tension for a given surface excess.

Another way of characterizing the localization of adsorbed polymers at the liquid–liquid interface, and correlating that with the reduction of interfacial tension, is to examine the crossing fraction $f_\times$ introduced in Sec. II D. The results are plotted in Fig. 6. The crossing fraction $f_\times$ changes dramatically with polymer sequence, with blockier copolymers crossing the interface on fewer occasions. For block copolymers, $f_\times \simeq 0.01$ for all values of the surface excess, showing that there are only about 1.3 interface crossings per molecule, on average, meaning mostly one crossing, and rarely three crossings. Gradient copolymers show much higher values of $f_\times$ that decrease with increasing surface excess. At low surface excess, the copolymers are able to adsorb at the interface to optimize interactions with the liquids. As the surface excess increases, the surface becomes crowded, which forces weakly bound segments to desorb from the interface, and reduces the fraction of bonds crossing the interface. Similar results are observed for the copolymer with $b = 1$. With higher values of b, and hence more blockiness, $f_\times$ is almost constant with increasing surface excess because the crowding effect is not important for copolymers aligned perpendicular to the interface. For a given surface excess, the more linear the composition profile (the smaller the value of b), the higher the polymer concentration at the interface, the more interface crossings, and the greater the reduction in the interfacial tension.

At this point, it is useful to connect the coarse-grained model with real systems. Yuan *et al.* compared the interfacial-tension reduction resulting from the adsorption of block and gradient copolymers at the water–chloroform interface.[26] The interfacial tension at the pure water–chloroform interface at $T = 25\,^\circ$C is 31.6 mN m^{-1}[47] or 30.8 mN m^{-1}.[48] In the coarse-grained simulations, the corresponding interfacial tension is $\gamma\sigma^2/\varepsilon \simeq 0.67$. Using rough estimates of $\sigma = 3$ Å and $\varepsilon = k_B T$, the real interfacial tension is $\gamma = 30.6$ mN m^{-1}. Yuan *et al.* measured the effects of block and gradient copolymers on the water–chloroform interfacial tension using drop shape analysis. For gradient copolymers, they reported values of γ in the range 16–21 mN m^{-1}, depending on the molecular weight and solution concentration of the copolymer.[26] These map on to reduced values of $\gamma^* = 0.35$–0.46, and from Fig. 5, this means polymer surface excesses $\Gamma^{ex}\sigma^2 = 0.02$–$0.03$. Unfortunately, the surface excesses have not been determined in experiments, and hence, this is an indirect comparison, but it does show that a reduction in interfacial tension, comparable to the experiment, is achievable with physically reasonable concentrations of adsorbed polymers. The equivalent experiments with block copolymers show very little effect on γ.[26] With the assumption that $\sigma = 3$ Å, and that one bead is equivalent to one acrylic-acid/styrene monomer, an estimated experimental surface excess of $\Gamma^{ex} = 1.6$ mg m^{-2} is roughly equivalent to a coarse-grained simulation of $\Gamma^{ex}\sigma^2 = 0.008$.[26] For gradient copolymers at this surface excess, the experimentally measured percentage decrease of γ is 8%, which is comparable to the decrease of 5% for the coarse-grained model.

Yuan *et al.* hypothesized that the lower surface activity of block copolymers is due to a lower critical micelle concentration, and a larger energy barrier associated with transferring a block copolymer from a micelle in solution to the interface.[26] This effect is not modeled here, as the solution concentration is zero, and the surface excess is prescribed. Nonetheless, the coarse-grained model demonstrates that when block copolymers adsorb at the interface, they have a much smaller impact on interfacial tension than do gradient copolymers. Yuan *et al.* also identified a "local segment desorption" mechanism for gradient copolymers.[26] As the polymer surface excess increases, short polymer segments desorb from

the interface to keep the monomer concentrations constant at the interface. This correlates well with the results shown in Fig. 6, as such desorption will also lead to fewer crossing points.

To summarize, gradient copolymers have been shown to form very different structures than block copolymers at the liquid–liquid interface, characterized by "parallel" and "perpendicular" alignments with the interface, respectively. The partial density profiles for the block copolymers show two separate peaks for each monomer type, and with minimal overlap. The corresponding peaks for gradient copolymers show significant overlap, leading to a single maximum at the interface. The different structures at the interface are shown to have substantial impacts on interfacial-tension reduction. At equivalent surface excesses, gradient copolymers are much more effective surfactants than block copolymers. The central finding is that the interfacial tension can be systematically changed by changing the monomer sequence.

B. All-atom simulations

Simulations of acrylic-acid/styrene copolymers at the water–chloroform interface at $T = 23\,^{\circ}\mathrm{C}$ were carried out for comparison with a previous experimental study.[26] Each interface had an area of approximately 10^4 Å^2. A simulation without polymers showed the expected phase separation, with the water and chloroform bulk densities equal to 1012 and 1499 kg m^{-3}, respectively. The corresponding interfacial tension was $\gamma = 40.97 \pm 0.20$ mN m^{-1}. This is significantly higher than the experimental values of 31.8 mN m^{-1} at $T = 23\,^{\circ}\mathrm{C}$[26] and 31.6 mN m^{-1} at $T = 25\,^{\circ}\mathrm{C}$,[47] but the main point of interest here will be the change in interfacial tension upon adding copolymers.

A single polymer consisted of 32 styrene monomer units and 32 acrylic-acid units, with a total mass of 5.6 kDa. Simulations were carried out with five polymers at each interface ($\Gamma^{ex} = 0.44$ mg m^{-2}) to examine the conformations of weakly interacting polymers, and with 20 polymers at each interface ($\Gamma^{ex} = 1.67$ mg m^{-2}) to accentuate differences in the resulting interfacial tension. Gradient copolymers ($b = 0$) are compared to block copolymers ($b = \infty$). Other simulation details are given in Sec. II B. Note that the simulated polymers are much shorter (by at least seven times) than those used in experiments.[26] The quantitative effects of this difference will be discussed specifically in Sec. III B 2.

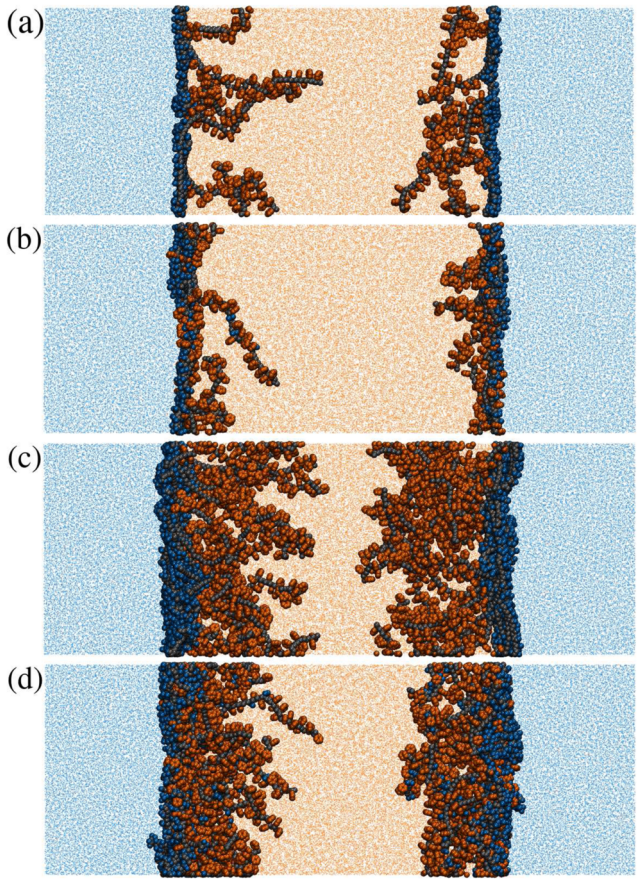

FIG. 7. Snapshots from all-atom simulations of acrylic-acid/styrene copolymers at the water–chloroform interface: (a) block copolymers, $\Gamma^{ex} = 0.44$ mg m^{-2}; (b) gradient copolymers, $\Gamma^{ex} = 0.44$ mg m^{-2}; (c) block copolymers, $\Gamma^{ex} = 1.67$ mg m^{-2}; (d) gradient copolymers, $\Gamma^{ex} = 1.67$ mg m^{-2}. The color scheme is as follows: carbon atoms on the phenyl ring of styrene—orange; carbon atoms on the backbone of styrene—gray; carbon atoms of acrylic acid—blue; water molecules—light blue; chloroform—light orange. Hydrogen atoms are omitted from the polymers for clarity.

1. Low surface excess

Figures 7(a) and 7(b) show snapshots from simulations with block and gradient copolymers at $\Gamma^{ex} = 0.44$ mg m^{-2}. The liquids separate into water-rich and chloroform-rich phases and with the polymers localized at the interfaces. With block copolymers, all of the acrylic-acid monomers adsorb at the interfaces, with the carboxylic acid moiety in contact with the water phase, and the polymer backbone oriented toward the chloroform phase. Each of these monomers, therefore, acts like a small surfactant, with the polar and non-polar parts solvated by the respective good solvents. The polystyrene segment of the block copolymer is fully solvated in the chloroform phase. The gradient copolymer does not extend as far into the chloroform phase as the block copolymer; in this case, most of the acrylic-acid monomers are strongly localized at the interface, except those surrounded by styrene monomers. The entropic penalty of adopting particular conformations with neighboring monomers in different solvents is too great. Moving along the chain from the acrylic-acid end to the styrene end, at some point, the balance shifts, and eventually, all of the styrene units can be fully solvated by the chloroform without penalty.

The polymer concentration profiles along the axis perpendicular to the interface are shown in Figs. 8(a) and 8(b). These represent the number of atoms per unit volume belonging to a particular monomer type, and the position of a monomer is taken to be that of the ipso carbon of styrene or the carbonyl carbon of acrylic acid. In the case of the block copolymer—Fig. 8(a)—all of the acrylic-acid units are adsorbed at the interface. The styrene units are solvated in chloroform and show a broad peak a short distance away from the interface. This behavior is similar to that of the coarse-grained model, as shown in Figs. 4(a) and 4(c). Turning to the solvents, and comparing Figs. 4(e) and 8(c), the chloroform mass-density profile resembles that of a coarse-grained solvent, with a local minimum in

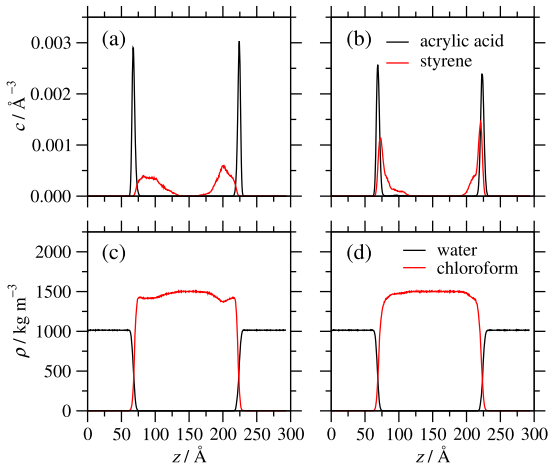

FIG. 8. Density profiles for monomers and solvent molecules from simulations of acrylic-acid/styrene copolymers at the water–chloroform interface with $\Gamma^{ex} = 0.44$ mg m^{-2}. (a) and (b) Concentration profiles (number of atoms per unit volume) for atoms in acrylic acid and styrene: (a) block copolymers and (b) gradient copolymers. (c) and (d) Mass-density profiles for the different solvents: (c) with block copolymers and (d) with gradient copolymers.

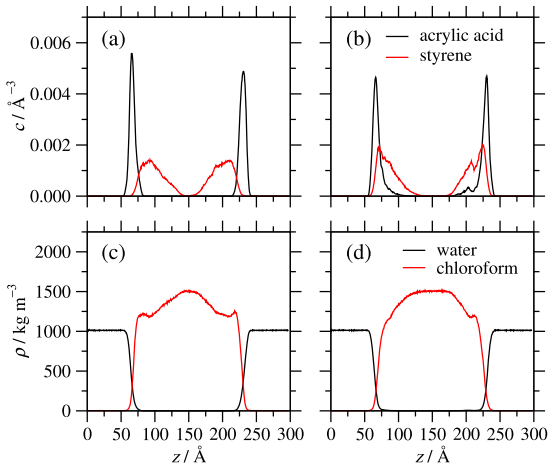

FIG. 9. Density profiles for monomers and solvent molecules from simulations of acrylic-acid/styrene copolymers at the water–chloroform interface with $\Gamma^{ex} = 1.67$ mg m^{-2}. (a) and (b) Concentration profiles (number of atoms per unit volume) for atoms in acrylic acid and styrene: (a) block copolymers and (b) gradient copolymers. (c) and (d) Mass-density profiles for the different solvents: (c) with block copolymers and (d) with gradient copolymers.

density at the position of the polymer peak, before approaching its bulk density in the middle of the layer. The water-rich phase does not show the same feature, as most of the acrylic-acid monomers are strongly localized at the interface.

Gradient copolymers—Fig. 8(b)—show a slightly smaller but broader acrylic-acid peak due to the interpolating styrene units. In the case where acrylic-acid units are completely surrounded by a styrene-rich segment of the polymer, desorption of these units is favored. An example of this desorption can be seen at the left-hand interface in Fig. 7(b), where a few acrylic-acid units (blue) are solvated in the chloroform phase (light orange). Larger differences are seen in the styrene concentration profiles. The acrylic-acid monomers pin the styrene monomers to the interface, giving sharp, almost coincident peaks in the concentration profile. Overall, the concentration of the gradient copolymers right at the interface is higher than that of the block copolymers, and this is the same behavior seen in the coarse-grained model, where different monomers hold each other close to the interface. The solvent mass-density profiles in Fig. 8(d) resemble the rounded profiles for the coarse-grained solvents in Fig. 4(f), except that the atomistic solvents have different mass densities.

2. High surface excess

Figures 7(c) and 7(d) show snapshots of the block and gradient copolymer simulations at $\Gamma^{ex} = 1.67$ mg m^{-2}. There are some similarities to the low-concentration case. With block copolymers, all acrylic-acid units are adsorbed at the interface, and all styrene monomers are solvated in the chloroform phase. The orientation of the carboxylic acid moiety toward the water phase and the hydrocarbon backbone toward the chloroform phase are less obvious as the surface crowding forces some monomers away from the interface. This has the effect of thickening the layer of acrylic acid. The gradient copolymer layer does not extend as far into the chloroform phase and is more concentrated at the interface due to the strong adsorption of the acrylic-acid units. There are more acrylic-acid segments dissolved in the chloroform phase than in the low surface concentration system, as there is a stronger entropic penalty of adsorption at the interface due to surface crowding.

The density profiles for the high surface concentration case are shown in Fig. 9. With block copolymers, all of the acrylic-acid units are adsorbed at the interface, and the styrene units are more fully solvated in chloroform. The chloroform density profile shows more pronounced minima near the interfaces due to the higher polymer density, and only a narrow slab at the bulk density between the interfaces. The water remains largely unaffected, as the acrylic-acid units are all adsorbed at the interface. Overall, apart from the scales, the profiles are qualitatively similar to those in the low surface concentration case.

The gradient copolymer density profile is somewhat similar to that in the low-concentration case, but there are some subtle differences. The acrylic-acid peak is broader due to styrene units competing for space at the interface, and it extends further into the chloroform phase. This partial desorption from the interface is due to crowding. This is in agreement with the proposed hypothesis of Yuan *et al.*,[26] that part of the gradient copolymer desorbs at higher surface concentrations in order to alleviate crowding. The chloroform density profile in Fig. 9(d) is more rounded than with the block copolymer due to the larger overlap of the monomer concentration peaks. There is a small minimum at $z \simeq 200$ Å, and a minor inflection at $z \simeq 100$ Å, which correspond to some transient structuring in the polymer layer.

The qualitative similarities in both the polymer and solvent density profiles at different surface concentrations are to be expected on the basis of what was found with the coarse-grained model. As shown in Fig. 4, changing Γ^{ex} makes the features of the density profile more pronounced, but it does not change their overall shape.

TABLE II. Simulated values of the interfacial tension for block and gradient acrylic-acid/styrene copolymers at the water–chloroform interface at different surface concentrations.

Γ^{ex}/mg m^{-2}	γ/mN m^{-1} block	γ/mN m^{-1} gradient
0.00	40.97 ± 0.20	40.97 ± 0.20
0.44	40.39 ± 0.21	39.38 ± 0.21
1.67	19.18 ± 0.25	10.90 ± 0.26

As with the coarse-grained model, the interfacial tension is affected by the presence of copolymers at the interface, and the different structures of the adsorbed films arising from the polymer architecture. The changes in interfacial tension with surface excess are summarized in Table II. With block copolymers, the interfacial tension drops by 1.4% with Γ^{ex} = 0.44 mg m^{-2}, and 53% with Γ^{ex} = 1.67 mg m^{-2}. With gradient copolymers, the corresponding drops are 3.9% and 73% at low and high surface concentrations, respectively. At low surface concentration, the gradient copolymer produces an almost three times larger reduction in γ than the block copolymer, but at high surface concentration, the difference is a factor of about 1.5. This may be connected with the fact that at low surface concentration, the acrylic acid in the gradient copolymer is very strongly pinned at the interface, and this leads to a high concentration of styrene there as well; see Fig. 8(b). With the block copolymer, the acrylic-acid and styrene peaks are quite well separated; see Fig. 8(a). At high surface concentration, crowding at the interface causes some desorption of the acrylic acid, and reduces the differences between the block and gradient concentration profiles; see Figs. 9(a) and 9(b). These differences in polymer concentration at the interface correlate with the relative changes in the interfacial tension.

Although the absolute values of the simulated interfacial tensions are not directly comparable to the experimental values, the relative changes can be used to gain useful insights. Yuan *et al.* showed that gradient copolymers at bulk concentrations of 0.1 mg ml^{-1} reduced the interfacial tension from 32 mN m^{-1} to 16 – 21 mN m^{-1}, depending on the molecular weight (38.6–91.8 kDa).[26] Block copolymers lead to much smaller decreases, on the order of a few mN m^{-1}. As noted in Sec. II A, this could be due to the lower critical micelle concentration of block copolymers, and less adsorption at the liquid–liquid interface. A gradient copolymer at 0.004 mg ml^{-1} gave an interfacial tension of about 29 mN m^{-1} (Fig. 4 of Ref. 26). Yuan *et al. estimated* that if all of the polymer adsorbed on a pendant drop of chloroform in water, then the surface excess would be 1.6 mg m^{-2}. The simulation of at Γ^{ex} = 1.67 mg m^{-2} showed a much larger decrease in interfacial tension than in the experiments, and this could be due to one or more factors. First, the surface excess in the experiment, which is undetermined, could be much less than that in the simulation, which is fixed. Second, there are large differences in the sizes of the polymers. The experiments are performed on polymers at least seven times longer than those in the simulations, and hence, the composition gradient is much less in real gradient copolymers. The same surface excess would be achieved experimentally with seven times fewer polymers, and more of each polymer would be solvated in the bulk liquids, hence reducing the concentration of monomers at the dividing surface between the two liquids. All of these effects could lead to the simulated polymers giving rise to larger changes in interfacial tension than those measured experimentally. Nonetheless, the qualitative agreement between the coarse-grained simulations of long polymers, and the atomistic simulations of short polymers, indicates that the structures and trends identified in both are correct.

It should also be noted that the acrylic-acid monomers simulated here are all in the neutral, protonated form. Yuan *et al.* performed experiments on copolymers at pH = 5.5.[26] Under these conditions, around 10% of the monomers in a poly(acrylic acid) homopolymer in an aqueous solution (pK_a = 4.26) dissociate to form the anionic conjugate base.[49] Dissociation can be inferred by monitoring changes in polymer conformation as a function of pH. This has been investigated using fluorescence spectroscopy, and it was found that for homopolymers below 16.5 kDa, there is no pH-dependent conformational change, whereas there is a coil-globule crossover for larger polymers.[49] This crossover is due to the degree of dissociation, and the relationship between the Bjerrum length (controlling the range of electrostatic repulsions) and the radius of gyration of the polymer. For short polymers, the conformation is always a coil, and the protonation state does not have a strong influence on polymer conformation. Therefore, for the 5.6 kDa polymers in this part of the study, and at pH = 5.5, it is a reasonable approximation to treat all of the monomers as being associated. It is possible that dissociation of some acrylic-acid monomers could change the polymer conformation at the interface,[25] but the presence of non-polar monomers in the copolymer, and a non-polar solvent at the interface, should, if anything, hinder charge separation.

IV. CONCLUSIONS

The effects of architecture on the properties of polymeric surfactants at liquid–liquid interfaces have been examined using molecular-dynamics simulations. The primary focus was on the differences between block copolymers and gradient copolymers. First, a coarse-grained, bead-spring model of the polymers was developed with a controlled level of blockiness, ranging from block to gradient. The interface was modeled using a non-additive binary Lennard-Jones liquid in its two-phase region. For a given surface excess, gradient copolymers lead to a greater reduction in interfacial tension than block copolymers. This is controlled by the extent to which the polymers are localized at the interface: a block copolymer is aligned preferentially perpendicular to the interface, with one crossing point, and each block fully solvated by the respective good solvent; in contrast, the central section of a gradient copolymer is strongly localized at the interface, there are multiple crossing points, and with only short sections at each end solvated in the bulk liquids. Hence, the reduction in interfacial tension is correlated with the total monomer concentrations at the interface. In more detail, the monomer-density profiles for the block copolymers display distinct peaks on either side of the interface, and with almost no overlap, while the gradient copolymers show a much greater density at the interface, and with significant overlap of the two monomer peaks. Results with varying levels of blockiness interpolate smoothly between the two extremes.

Some all-atom simulations of acrylic-acid/styrene copolymers at the water–chloroform interface were carried out to test the

predictions from the coarse-grained model, and to compare to existing experiments.[26] Once again, the gradient copolymer was found to reduce the interfacial tension more than the block copolymer, for a given surface excess. In many respects, the density profiles for the polymers and solvents strongly resemble those from the coarse-grained modeling, confirming the reliability of the predictions from the latter. The qualitative agreement between the coarse-grained and all-atom simulations shows that the relevant molecular-scale features are captured in a simple model. The energy parameters given in Table I, and the common bead diameter σ, are the simplest possible choices, with complete symmetry between the A and B species in both the solvents and the copolymers. In fact, the parameter space is large, and it is likely that appropriate values could be found for accurate, large-scale, coarse-grained simulations of a particular system. This would take a lot of effort and is beyond the scope of this exploratory study.

The surface excess was controlled in the simulations, which eliminates any differences in bulk-solution self-assembly, critical micelle concentration, and adsorption kinetics arising from changing the polymer architecture. Therefore, the differences revealed by the simulations arise from how the polymers are structured at the liquid–liquid interface. This sheds light on how architecture (as opposed to chemical composition) can be used to fine-tune the interfacial properties of polymeric surfactants at liquid–liquid interfaces.

ACKNOWLEDGMENTS

This research was supported jointly by Infineum UK Ltd. and the Engineering and Physical Sciences Research Council (Project Reference EP/T517884/1) through a studentship for J. G. C. For the purpose of open access, the authors have applied a Creative Commons Attribution (CC BY) license to any Author Accepted Manuscript version arising from this submission.

AUTHOR DECLARATIONS

Conflict of Interest

The authors have no conflicts to disclose

Author Contributions

Jonathan G. Coldstream: Conceptualization (equal); Data curation (lead); Formal analysis (equal); Investigation (lead); Methodology (equal); Software (lead); Validation (lead); Visualization (lead); Writing – original draft (equal); Writing – review & editing (equal). **Philip J. Camp**: Conceptualization (equal); Formal analysis (equal); Funding acquisition (equal); Methodology (equal); Project administration (lead); Resources (lead); Supervision (equal); Writing – original draft (equal); Writing – review & editing (equal). **Daniel J. Phillips**: Conceptualization (equal); Supervision (equal); Writing – review & editing (equal). **Peter J. Dowding**: Conceptualization (equal); Funding acquisition (equal); Supervision (equal); Writing – review & editing (equal).

DATA AVAILABILITY

The data that support the findings of this study are available from the corresponding author upon reasonable request.

REFERENCES

[1] I. Kralova and J. Sjöblom, "Surfactants used in food industry: A review," J. Dispersion Sci. Technol. **30**, 1363–1383 (2009).
[2] J. J. Scheibel, "The evolution of anionic surfactant technology to meet the requirements of the laundry detergent industry," J. Surfactants Deterg. **7**, 319–328 (2004).
[3] H. Spikes, "Friction modifier additives," Tribol. Lett. **60**, 5 (2015).
[4] O. Massarweh and A. S. Abushaikha, "The use of surfactants in enhanced oil recovery: A review of recent advances," Energy Rep. **6**, 3150–3178 (2020).
[5] Y. Chen, H. Chen, M. Feng, and Y. Dong, "Amphiphilic gradient copolymers: Synthesis, self-assembly, and applications," Eur. Polym. J. **85**, 489–498 (2016).
[6] Z. Zheng, X. Gao, Y. Luo, and S. Zhu, "Employing gradient copolymer to achieve gel polymer electrolytes with high ionic conductivity," Macromolecules **49**, 2179–2188 (2016).
[7] S. Wang, L. Zhang, A. Wang, X. Liu, J. Chen, Z. Wang, Q. Zeng, H. Zhou, X. Jiang, and L. Zhang, "Polymer-laden composite lignin-based electrolyte membrane for high-performance lithium batteries," ACS Sustain. Chem. Eng. **6**, 14460–14469 (2018).
[8] C. Lefay, B. Charleux, M. Save, C. Chassenieux, O. Guerret, and S. Magnet, "Amphiphilic gradient poly(styrene-co-acrylic acid) copolymer prepared via nitroxide-mediated solution polymerization. synthesis, characterization in aqueous solution and evaluation as emulsion polymerization stabilizer," Polymer **47**, 1935–1945 (2006).
[9] S. R. George, C. A. Sanders, G. A. Deeter, J. D. Campbell, B. Reck, and M. F. Cunningham, "Amphiphilic block-random copolymer stabilizers: A 'seeded coagulative' emulsion polymerization mechanism," Macromolecules **55**, 5279–5290 (2022).
[10] F. Perin, A. Motta, and D. Maniglio, "Amphiphilic copolymers in biomedical applications: Synthesis routes and property control," Mater. Sci. Eng.: C **123**, 111952 (2021).
[11] J. D. Jang, Y.-J. Yoon, S.-W. Jeon, Y. S. Han, and T.-H. Kim, "Molecular weight-dependent, flexible phase behaviors of amphiphilic block copolymer/additive complexes in aqueous solution," Polymers **13**, 178 (2021).
[12] K. E. B. Doncom, L. D. Blackman, D. B. Wright, M. I. Gibson, and R. K. O'Reilly, "Dispersity effects in polymer self-assemblies: A matter of hierarchical control," Chem. Soc. Rev. **46**, 4119–4134 (2017).
[13] R. F. G. Apóstolo, P. J. Camp, B. N. Cattoz, P. J. Dowding, and A. D. Schwarz, "Effect of functional-group distribution on the structure of a polymer in non-aqueous solvent," Mol. Phys. **116**, 2942–2953 (2018).
[14] J. G. Coldstream, P. J. Camp, D. Phillips, and P. J. Dowding, "Gradient copolymers versus block copolymers: Self-assembly in solution and surface adsorption," Soft Matter **18**, 6538–6549 (2022).
[15] J. Kim, M. M. Mok, R. W. Sandoval, D. J. Woo, and J. M. Torkelson, "Uniquely broad glass transition temperatures of gradient copolymers relative to random and block copolymers containing repulsive comonomers," Macromolecules **39**, 6152–6160 (2006).
[16] M. M. Mok, J. Kim, and J. M. Torkelson, "Gradient copolymers with broad glass transition temperature regions: Design of purely interphase compositions for damping applications," J. Polym. Sci., Part B: Polym. Phys. **46**, 48–58 (2008).
[17] S. Okabe, K. Seno, S. Kanaoka, S. Aoshima, and M. Shibayama, "Micellization study on block and gradient copolymer aqueous solutions by DLS and SANS," Macromolecules **39**, 1592–1597 (2006).
[18] S. Okabe, K. Seno, S. Kanaoka, S. Aoshima, and M. Shibayama, "Small-angle neutron scattering study on block and gradient copolymer aqueous solutions," Polymer **47**, 7572–7579 (2006).
[19] M. D. Lefebvre, M. Olvera de la Cruz, and K. R. Shull, "Phase segregation in gradient copolymer melts," Macromolecules **37**, 1118–1123 (2004).
[20] M. D. Lefebvre, C. M. Dettmer, R. L. McSwain, C. Xu, J. R. Davila, R. J. Composto, S. T. Nguyen, and K. R. Shull, "Effect of sequence distribution on copolymer interfacial activity," Macromolecules **38**, 10494–10502 (2005).
[21] S. Jouenne, J. A. González-León, A. Ruzette, P. Lodefier, S. Tencé-Girault, and L. Leibler, "Styrene/butadiene gradient block copolymers: Molecular and mesoscopic structures," Macromolecules **40**, 2432–2442 (2007).

[22]J. Kim, M. K. Gray, H. Zhou, S. T. Nguyen, and J. M. Torkelson, "Polymer blend compatibilization by gradient copolymer addition during melt processing: Stabilization of dispersed phase to static coarsening," Macromolecules **38**, 1037–1040 (2005).
[23]J. L. Self, A. J. Zervoudakis, X. Peng, W. R. Lenart, C. W. Macosko, and C. J. Ellison, "Linear, graft, and beyond: Multiblock copolymers as next-generation compatibilizers," JACS Au **2**, 310–321 (2022).
[24]C. L. H. Wong, J. Kim, C. B. Roth, and J. M. Torkelson, "Comparison of critical micelle concentrations of gradient copolymer and block copolymer in homopolymer: Novel characterization by intrinsic fluorescence," Macromolecules **40**, 5631–5633 (2007).
[25]F. Jiménez-Ángeles, H. Kwon, K. Sadman, T. Wu, K. R. Shull, and M. Olvera de la Cruz, "Self-assembly of charge-containing copolymers at the liquid–liquid interface," ACS Cent. Sci. **5**, 688–699 (2019).
[26]W. Yuan, M. M. Mok, J. Kim, C. L. H. Wong, C. M. Dettmer, S. T. Nguyen, J. M. Torkelson, and K. R. Shull, "Behavior of gradient copolymers at liquid/liquid interfaces," Langmuir **26**, 3261–3267 (2010).
[27]W. L. Jorgensen, J. D. Madura, and C. J. Swenson, "Optimized intermolecular potential functions for liquid hydrocarbons," J. Am. Chem. Soc. **106**, 6638–6646 (1984).
[28]W. L. Jorgensen, D. S. Maxwell, and J. Tirado-Rives, "Development and testing of the OPLS all-atom force field on conformational energetics and properties of organic liquids," J. Am. Chem. Soc. **118**, 11225–11236 (1996).
[29]S. W. I. Siu, K. Pluhackova, and R. A. Böckmann, "Optimization of the OPLS-AA force field for long hydrocarbons," J. Chem. Theory Comput. **8**, 1459–1470 (2012).
[30]G. S. Grest and K. Kremer, "Molecular dynamics simulation for polymers in the presence of a heat bath," Phys. Rev. A **33**, 3628–3631 (1986).
[31]P. G. de Gennes, *Scaling Concepts in Polymer Physics*, 1st ed. (Cornell University Press, Ithaca, 1979).
[32]G. S. Grest, K. Kremer, and T. A. Witten, "Structure of many arm star polymers: A molecular dynamics simulation," Macromolecules **20**, 1376–1383 (1987).
[33]G. S. Grest, M.-D. Lacasse, K. Kremer, and A. M. Gupta, "Efficient continuum model for simulating polymer blends and copolymers," J. Chem. Phys. **105**, 10583–10594 (1996).
[34]K. Binder, J. Baschnagel, and W. Paul, "Glass transition of polymer melts: Test of theoretical concepts by computer simulation," Prog. Polym. Sci. **28**, 115–172 (2003).
[35]C. Svaneborg and R. Everaers, "Characteristic time and length scales in melts of Kremer–Grest bead–spring polymers with wormlike bending stiffness," Macromolecules **53**, 1917–1941 (2020).
[36]A. Chremos, E. Glynos, V. Koutsos, and P. J. Camp, "Adsorption and self-assembly of linear polymers on surfaces: A computer simulation study," Soft Matter **5**, 637–645 (2009).
[37]A. Chremos, P. J. Camp, E. Glynos, and V. Koutsos, "Adsorption of star polymers: Computer simulations," Soft Matter **6**, 1483–1493 (2010).
[38]D. S. Wood, V. Koutsos, and P. J. Camp, "Computer simulations of surface deposition of amphiphilic diblock copolymers driven by solvent evaporation," Soft Matter **9**, 3758–3766 (2013).
[39]B. Dünweg and K. Kremer, "Molecular dynamics simulation of a polymer chain in solution," J. Chem. Phys. **99**, 6983–6997 (1993).
[40]M. P. Taylor, W. Paul, and K. Binder, "Applications of the Wang–Landau algorithm to phase transitions of a single polymer chain," Polym. Sci. Ser. C **55**, 23–38 (2013).
[41]S. Roy, S. Dietrich, and F. Höfling, "Structure and dynamics of binary liquid mixtures near their continuous demixing transitions," J. Chem. Phys. **145**, 134505 (2016).
[42]L. Martínez, R. Andrade, E. G. Birgin, and J. M. Martínez, "PACKMOL: A package for building initial configurations for molecular dynamics simulations," J. Comput. Chem. **30**, 2157–2164 (2009).
[43]LAMMPS Molecular Dynamics Simulator, http://www.lammps.org (2023).
[44]S. Plimpton, "Fast parallel algorithms for short-range molecular dynamics," J. Comput. Phys. **117**, 1–19 (1995).
[45]A. P. Thompson, H. M. Aktulga, R. Berger, D. S. Bolintineanu, W. M. Brown, P. S. Crozier, P. J. in 't Veld, A. Kohlmeyer, S. G. Moore, T. D. Nguyen, R. Shan, M. J. Stevens, J. Tranchida, C. Trott, and S. J. Plimpton, "LAMMPS – a flexible simulation tool for particle-based materials modeling at the atomic, meso, and continuum scales," Comput. Phys. Commun. **271**, 108171 (2022).
[46]J. S. Rowlinson and B. Widom, *Molecular Theory of Capillarity* (Dover Publications Inc., Mineola, NY, 2002).
[47]D. J. Donahue and F. E. Bartell, "The boundary tension at water-organic liquid interfaces," J. Phys. Chem. **56**, 480–484 (1952).
[48]H. M. Backes, M. Jing Jun, E. Bender, and G. Maurer, "Interfacial tensions in binary and ternary liquid-liquid systems," Chem. Eng. Sci. **45**, 275–286 (1990).
[49]T. Swift, L. Swanson, M. Geoghegan, and S. Rimmer, "The pH-responsive behaviour of poly(acrylic acid) in aqueous solution is dependent on molar mass," Soft Matter **12**, 2542–2549 (2016).